*38th International Electric Vehicle Symposium and Exhibition (EVS38)*
*Göteborg, Sweden, June 15-18, 2025*

# Low-cost adaptation of electric vehicles to a test bench with wheel load machines

Markus Harke[1], Christian Dobhan[1], Andreas Daberkow[1],
[1]*Heilbronn University of Applied Sciences, Max-Planck-Str. 39, 74081 Heilbronn, Germany,*
*markus.harke@hs-heilbronn.de*

**Executive Summary**

Virtual product development of electric vehicles should avoid extensive testing of vehicles on test tracks and test benches. Nevertheless, selected prototype vehicles must still be tested in the product development process. New driver assistance systems further increase the cost of test bench analysis of complete vehicles. This article presents a new cost-effective and space-saving adaptation of vehicles to a test bench for the electric drivetrain. The multifunctional support bearings developed allow a space-saving setup and quick adaptation. The article presents the test bench setup and initial tests for an electric vehicle.

*Keywords: Measuring Methods & Equipment, Electric Vehicles, Vehicle-in-the-Loop Testing, Dynamometer, Test Bench*

## 1 Introduction

In addition to classic roller test benches, test rigs in which wheel load machines simulate the wheel-road contact have also become established for testing complete vehicles. To do this, the driving wheels are unscrewed from the vehicle and the wheel hubs are connected to the wheel load machines. Originally, this type of testing originated from powertrain testing [1]. Compared with roller dynamometers, the vehicle test with wheel load machines is less expensive on account of the noticeably smaller space requirement. Moreover, it allows the measurement of a complete map of the electric drive unit [2]. In addition, the test rig with wheel load machines also allows dynamic driving manoeuvres with wheel-individual behaviour thanks to their low mass moment of inertia. Due to the superior dynamics this type of test rig is also a good choice for testing autonomous vehicles [3]. Vehicle approval still requires tests on the roller dynamometer. However, it has been shown for combustion-powered vehicles that it makes no difference in terms of consumption and emissions on which type of test rig the results are obtained [4][5]. It is to be expected that this also applies to electric cars. In order to be able to drive the electric vehicle under test (VUT) on a test bench with wheel load machines, the driving wheel axles of the VUT must be connected to the wheel load machines without the weight of the vehicle resting on these. The wheel suspension must be sprung in as if the vehicle were on the road so that the axle angles are correct. The market offers various solutions for this:

- Bearing blocks: each driven wheel hub of the VUT is connected to a connecting shaft which is guided in a bearing block. The bearing blocks support the weight of the vehicle. About a driveshaft, the connecting shaft is connected to the shaft of the wheel load machine [6]. To facilitate alignment, the driveshafts must be long. The wheel load machines are then far apart and the space required is large. Special solutions exist for the emulation of steering motions, but this additional feature entails long-travel CV joints and the demand for space on both sides of the VUT is really huge [7][8].

- Test wheels: Special test wheels are fitted instead of the original wheels. These contain a connecting shaft pivoted in the rim, which is connected to the wheel hub of the vehicle on one side and to the wheel load machine on the other side via a driveshaft. In test mode, only the connecting shaft rotates. The rim with the rubber tyre on it stands still. The advantage is that the contact conditions for the vehicle are very similar to those on the road. To make it easy to drive the VUT into the test stand, the connecting shaft can be firmly connected to the rim using a blocking device [9][10]. Wheel and rim sizes vary from vehicle to vehicle. A suitable test wheel is required for every vehicle. For service providers in particular, who want to test many different vehicles from different manufacturers, test wheels are therefore an expensive solution.
- Vehicle support on the wheel carriers: Suitable brackets support the vehicle weight directly on the wheel carriers. The wheel hubs of the VUT are connected to the wheel load machines via hub adapters and driveshafts [11]. This variant requires an individual bracket for each VUT. There must be a corresponding connection surface for the brackets on the underside of the wheel carrier of the VUT. This type of mounting is very vehicle-specific and is rarely used.
- Hub coupled dynamometers: this is a special system that combines the load machine, the sensors for wheel speed and wheel torque and the bearing to support the vehicle weight in a mobile structural unit. The manufacturers promise short set-up times [12] [13]. The load machine may be a hydraulic absorption unit or an electrical machine. Hydraulic load machines have an advantage because of their compact size [14]. For testing of electric vehicles they are not recommended yet, because the load machines must act as a motor if the VUT is recuperating. The VUT may even be able to perform steering movements [15]. Hub coupled dynamometers may be convincing for the conceptual design of a new test bench. But they are too expensive for anyone who already owns wheel load machines or would like to upgrade an existing powertrain test bench.

This paper presents a solution based on the principle of bearing blocks. Thanks to short driveshafts, it guarantees a space-saving design and still allows easy alignment and mounting of the VUT. Integrated buffers decouple the vehicle vibrations from the bed plate during the test. The next chapter presents the design. This is followed by a consideration of how the operator can use measurements to draw conclusions about the loads on the supports and their service life. Finally, the test bench operation of an exemplary vehicle is shown with the aid of the developed bearing. The test bench is used for research assignments as well as for comparisons of simulations and test runs within master courses in the sense of research-oriented learning [16].

## 2 Construction of the supports

Space requirement means costs. Cost-effective adaptation means that the distance between the VUT and wheel load machines must be small. For this reason, a short constant velocity driveshaft is used between the wheel load machine and the bearing block, which can only compensate for small misalignments. The VUT must therefore be positioned precisely. The design of the supports must enable a precise positioning in a simple manner. Fig. 1(a) illustrates one support. It consists of the substructure A, which is tightly

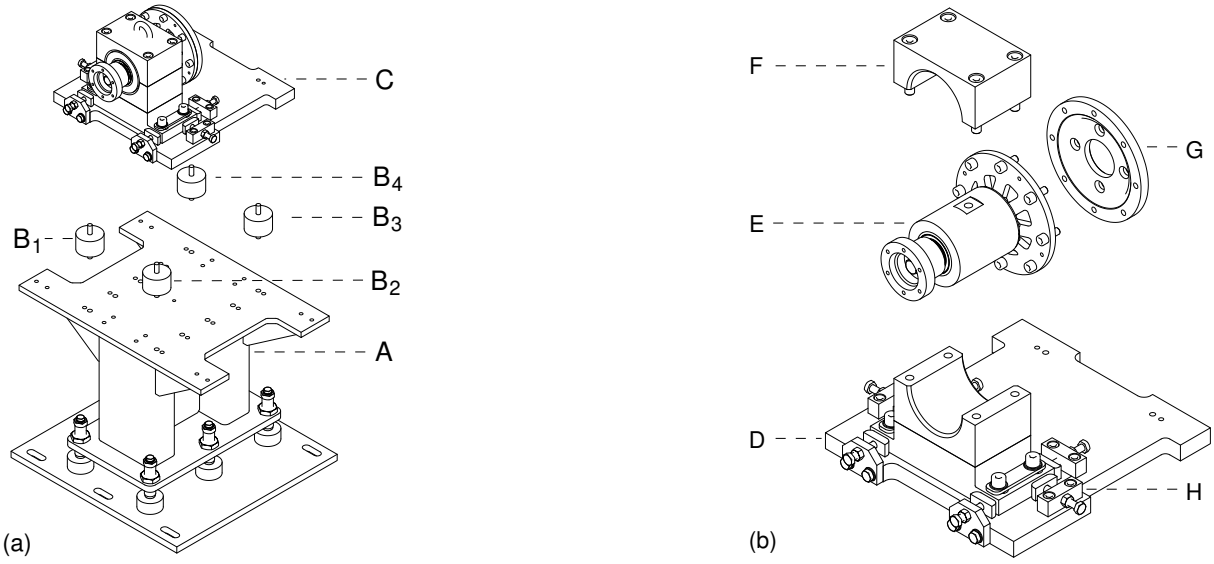


Figure 1: (a) Support and (b) vehicle mount

mounted on the T-slot plate of the test bench, and the vehicle mount C, via which the VUT is coupled to the wheel load machine. The vehicle mount and substructure are decoupled from each other via four rubber buffers $B_1 \ldots B_4$. These rubber buffers can be loaded in compression and in thrust, but never in tension. In order to prevent this undesirable tensile load, care was taken to ensure that the point at which the VUT introduces its forces and torques is centred between the four buffers of a support. This constraint explains the choice of width and depth of the support. Its height results from the fixed shaft height of the wheel load machines.
The vehicle mount in Fig. 1(b) has a multi-part structure to enable simple adjustment and mounting of the VUT. It consists of a supporting plate D with a bearing block lower part on it, the bearing housing E, which holds the output shaft, the bearing block upper part F and an adapter flange G between the wheel hub and the output shaft. This adapter flange must be made to fit the VUT because the rim connection to the wheel hub is vehicle-specific. Table 1 shows the rim specifications of some electric vehicles from the lower to middle segment. It can be seen that there are no uniform designs among the various manufacturers. All other parts apart from this adapter flange are independent of the VUT.

Table 1: Rim specifications of different electric vehicles

| Vehicle model | pitch circle diameter (mm) / No of holes | center bore (mm) | wheel mounting | tightening torque (Nm) |
|---|---|---|---|---|
| BYD Dolphin | 114,3 / 5 | 60,1 | lug nuts M12x1,5 | 120 |
| Dacia Spring ELECTRIC | 100 / 4 | 60,1 | wheel bolts M12x1,5 | 110 |
| Hyundai IONIQ 5 | 114,3 / 5 | 67,1 | wheel bolts M12x1,5 | 125 |
| NIO ET5 | 120 / 5 | 62,6 | wheel bolts M14x1,5 | 140 |
| Opel Corsa electric | 108 / 4 | 65,1 | wheel bolts M12x1,25 | 120 |
| Renault R5 E-TECH | 114,3 / 5 | 66,1 | wheel bolts M12x1,5 | 120 |
| VW ID.3 | 112 / 5 | 57,1 | wheel bolts M14x1,5 | 120 |

The substructure A consists of a base plate and a pedestal. The pedestal is connected to the base plate using floor levelling screws, which allow to adjust the height of the support slightly and permit minimal angular compensation.

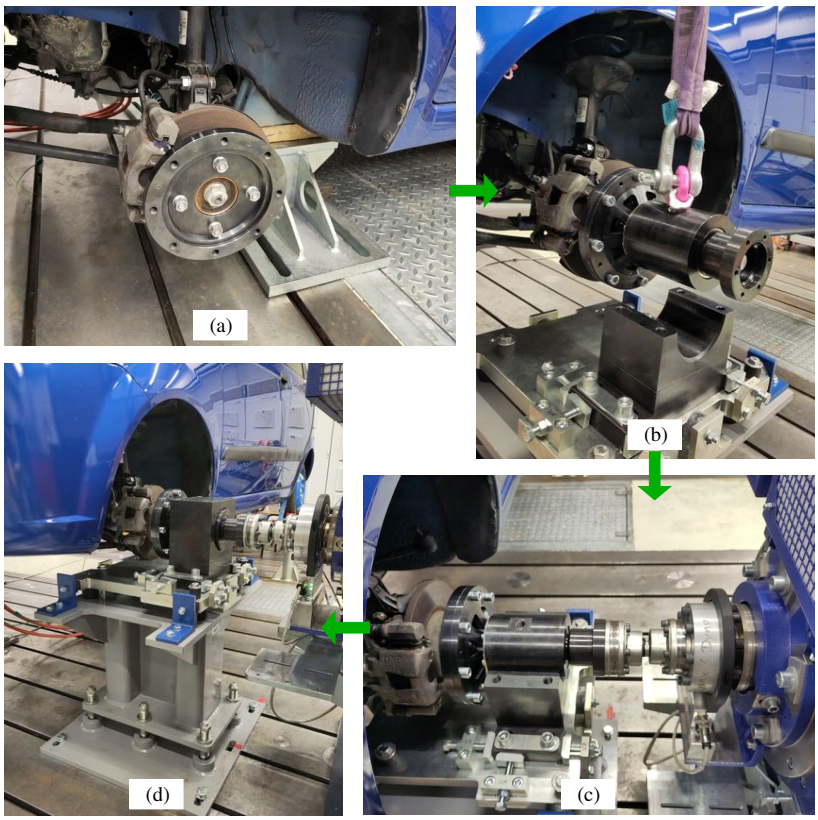


Figure 2: Mounting the VUT: (a) Adapter flange G on the VUT, (b) Inserting VUT into the bearing block lower part, (c) drive shafts inserted, (d) final assembly

The following description of the mechanical adaptation of a VUT on the test bench is based on the assumption that the VUT has one driving axle, so that two supports and two wheel load machines are sufficient. In order to accommodate a VUT on the test bench, the operator first has to align the supports with the wheel load machines in such a way that no large misalignment is to be expected after the insertion of the VUT: in the final position the flanges of the drive shafts should be as parallel to each other as possible. Then, he jacks up the VUT on the drive axle and removes the wheels. Instead of the wheels, the adapter flanges G are fitted to the wheel hubs of the VUT (Fig. 2(a)). Now remove the bearing block upper parts F and attach the output shafts with bearing housings E to the adapter flanges. Using eyebolts screwed into the bearing housings, the VUT can be raised on its drive axle and then lowered so that the bearing housings slide into the bearing block lower parts (Fig. 2(b)). This automatically aligns the VUT. Now the other axle of the VUT is jacked up and the alignment of the drive axle is checked after the drive shafts have been provisionally fitted (Fig. 2(c)). If there is too much misalignment on the drive shafts, the drive axle is lifted out of the bearing block lower parts again. Thus, the positions of the supports (or the VUT) can be slightly adjusted again: the height adjustment is made via the floor leveling screws. Fine positioning H allows adjustment in a horizontal direction. If the offset is within the tolerance after inserting the drive axle, the bearing block upper parts F are fitted. The output shafts can then be connected to the wheel load machines via the drive shafts (Fig. 2(d)).

# 3 Load and endurance

In addition to the weight of the vehicle, a mounted VUT causes additional clamping forces and torques on the supports, which are initially unknown to the operator and have a negative influence on the endurance of the support bearings. These clamping forces and torques can be determined as follows: dial gauges are used to record the movement of the supporting plate when the VUT is inserted. Thanks to a description of the kinematics of this support plate, the movement at the buffers can be deduced. Using the known spring constants of the buffers for compression and shear loads, the buffer forces can be derived. The following forces and torques can be calculated using suitable free-body diagrams of the vehicle mount:

- the vertical force $F_v$ transmitted from the vehicle to the support, which corresponds to the proportion of the weight that this support has to carry,
- the longitudinal force $F_l$ and lateral force $F_q$ applied to the supports by the vehicle,
- the track torque $M_{sp}$ and the camber torque $M_{st}$ caused by the mounted vehicle.

The bearing forces are determined on the basis of a free-body diagram of the output shaft. Knowing these gives the bearing service life.

## 3.1 Forces and torques on the vehicle mount

The calculation of the forces and torques on the vehicle mount is based on free-body diagrams, which are illustrated in Fig. 3. In it, green color marks forces and torques which the VUT exerts on the vehicle mount. The red labels $B_1 \ldots B_4$ mark the position of the four buffers. The buffer force components have the index $x$ in the direction of travel, the index $y$ transverse to the direction of travel and the index $z$ in the vertical direction.

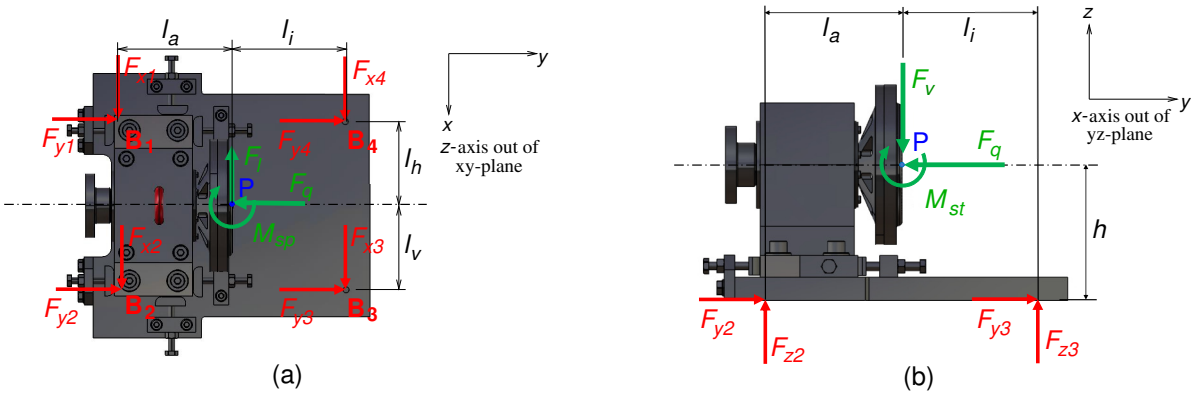


Figure 3: Free-body diagrams of the vehicle mount: (a) xy-plane, (b) yz-plane

From the free-body diagram of the vehicle mount in the xy-plane in Fig. 3(a) you get the longitudinal and transverse forces applied by the vehicle, which result from the buffer forces in the longitudinal and transverse directions:

$$F_l = F_{x1} + F_{x2} + F_{x3} + F_{x4} \ , \qquad F_q = F_{y1} + F_{y2} + F_{y3} + F_{y4} \tag{1}$$

The track torque $M_{sp}$ also follows from the sum of the moments at point P around the z-axis using this free-body diagram:

$$M_{Sp} = (F_{y2} + F_{y3}) \cdot l_v - (F_{y1} + F_{y4}) \cdot l_h + (F_{x1} + F_{x2}) \cdot l_a - (F_{x3} + F_{x4}) \cdot l_i \tag{2}$$

Fig. 3(b) shows a free-body diagramm of the vehicle mount in the yz-plane. Due to the view from the front, the forces of the rear buffers 1 and 4 are not visible. The vertical force $F_v$ which the vehicle acts on the support corresponds to the sum of the buffer vertical forces:

$$F_v = F_{z1} + F_{z2} + F_{z3} + F_{z4} \tag{3}$$

The sum of the moments at point P around the x-axis is used to calculate the camber torque $M_{St}$, which the clamped vehicle applies:

$$M_{St} = -(F_{z1} + F_{z2}) \cdot l_a + (F_{z3} + F_{z4}) \cdot l_i + (F_{y1} + F_{y2} + F_{y3} + F_{y4}) \cdot h \tag{4}$$

## 3.2 Bearing forces and endurance

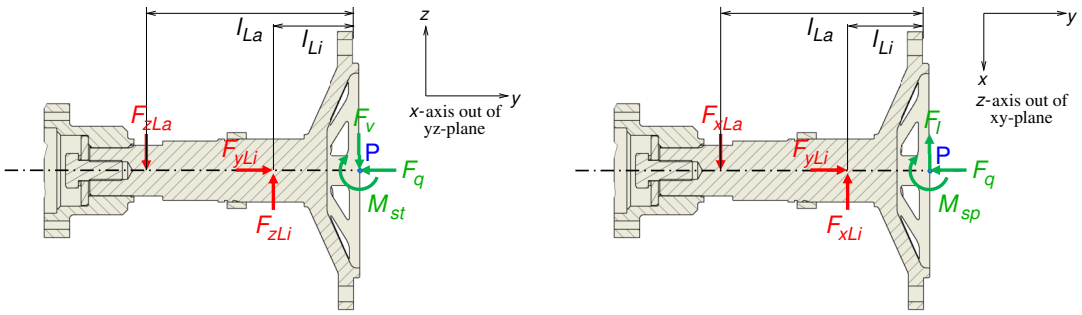


Figure 4: Free-body diagrams of the output shaft: left in yz-plane, right in xy-plane

The free-body diagrams of the output shaft in Fig. 4 allow the bearing forces to be calculated. Green color again marks forces and torques which the VUT acts on the output shaft. The reaction forces in the bearings appear in red color. The inner bearing is designed as a fixed bearing. It therefore also absorbs a force in the $y$-direction, which acts as an axial force on this bearing and corresponds to the transverse force applied by the VUT. The outer bearing is designed as a floating bearing. The bearing forces in the $z$-direction are obtained from the left-hand free-body diagram in Fig. 4 by setting up the force equilibrium in the $z$-direction and the sum of the moments at point P around the x-axis and solving these two equations for the bearing force components:

$$F_{zLi} = \frac{M_{St} + F_v \cdot l_{La}}{l_{La} - l_{Li}} \ , \qquad F_{zLa} = F_{zLi} - F_v \tag{5}$$

The right-hand free-body diagram in Fig. 4 is used to determine the bearing force components in the $x$-direction. To do this, formulate the force equilibrium in the $x$-direction and the sum of moments at point P about the z-axis and solve these two equations for the required force components:

$$F_{xLi} = \frac{M_{Sp} - F_l \cdot l_{La}}{l_{La} - l_{Li}} \ , \qquad F_{xLa} = F_{xLi} + F_l \tag{6}$$

The above force components result in the radial and axial force of the inner fixed bearing and the radial force of the outer floating bearing.

$$F_{r,i} = \sqrt{F_{xLi}^2 + F_{zLi}^2}, \quad F_{ax,i} = F_q, \qquad F_{r,a} = \sqrt{F_{xLa}^2 + F_{zLa}^2} \tag{7}$$

Hence, the dynamic equivalent bearing load and the endurance are calculated in accordance with the DIN standard [17] by means of the data sheet information on the bearings.

### 3.3 Movement of the supporting plate and buffer forces

The calculation of the load applied by the VUT in chapter 3.1 requires knowledge of the forces transmitted by the buffers. These can be determined by measuring the relative movement of the supporting plate when the VUT is inserted. The support plate is assumed to be rigid. The horizontal movement, which is responsible for the longitudinal and transverse forces at the buffers, is virtually independent of the height movement of the plate. This movement in the $xy$-plane is conceptually decomposed into a rotation by the angle $\alpha$ around its center point M and a shifting of the center point by the vector $\vec{S}$. Fig. 5 illustrates the approach by means of a simplified plate contour. For the sake of convenience, the reference system is set into the middle of the plate. Black color marks the original position of the plate and blue color marks the final position after insertion of the vehicle.

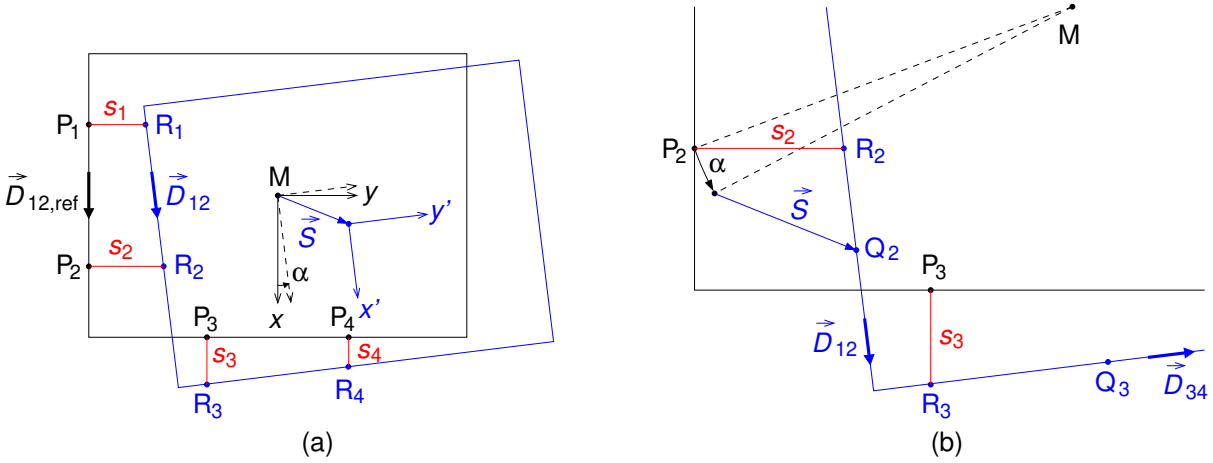


Figure 5: Horizontal movement of the supporting plate: (a) whole plate, (b) zoom to front outside corner

Dial gauges measure the distances $s_n$ shown in red while the vehicle is inserted. Their probe tips are located in the starting position at points $P_n$ and in the end position at points $R_n$. At least three dial gauges are necessary in order to record completely the plate movement in the horizontal plane. The fourth dial indicator is optional. The position vectors $\vec{R}$ for the end position follow with the measured distances $s_n$ from the known coordinates of the starting position.

$$\vec{R}_1 = \begin{pmatrix} x_{P1} \\ y_{P1} + s_1 \end{pmatrix} \quad \vec{R}_2 = \begin{pmatrix} x_{P2} \\ y_{P2} + s_2 \end{pmatrix} \quad \vec{R}_3 = \begin{pmatrix} x_{P3} + s_3 \\ y_{P3} \end{pmatrix} \quad \vec{R}_4 = \begin{pmatrix} x_{P4} + s_4 \\ y_{P4} \end{pmatrix} \tag{8}$$

#### 3.3.1 Determination of the plate rotation

For rotation angle $\alpha$, observe a plate edge: its direction vectors $\vec{D}_{12,ref}$ in the starting position and $\vec{D}_{12}$ in the end position are calculated using the position vectors $\vec{P}$ and $\vec{R}$.

$$\vec{D}_{12,ref} = \frac{\vec{P}_2 - \vec{P}_1}{|\vec{P}_2 - \vec{P}_1|} \qquad \vec{D}_{12} = \frac{\vec{R}_2 - \vec{R}_1}{|\vec{R}_2 - \vec{R}_1|} \tag{9}$$

The angle of rotation results from the scalar product of the two direction vectors:

$$\alpha = \arccos(\vec{D}_{12,ref} \cdot \vec{D}_{12}) \tag{10}$$

#### 3.3.2 Determination of the plate displacement

Fig. 5(b) shows a zoom of the outside front corner during the horizontal movement of the plate. The point $P_2$, at which the probe tip of the second dial gauge rests in the initial position, is mapped onto the point $Q_2$ by rotating it by the angle $\alpha$ and then shifting it by the vector $\vec{S}$:

$$\vec{Q}_2 = R(\alpha)\vec{P}_2 + \vec{S} \qquad \text{Rotation matrix } R(\alpha) = \begin{bmatrix} \cos\alpha & -\sin\alpha \\ \sin\alpha & \cos\alpha \end{bmatrix} \tag{11}$$

The probe tip of the dial gauge slides on the left edge of the plate as the plate moves. In the end position, it is located at point $R_2$, whose position vector is described by a straight line equation with reference point $Q_2$ and direction vector $\vec{D}_{12}$ and the parameter $m_2 \in \mathbb{R}$:

$$\vec{R}_2 = \vec{Q}_2 + m_2\vec{D}_{12} = R(\alpha)\vec{P}_2 + \vec{S} + m_2\vec{D}_{12} \tag{12}$$

In order to get the displacement vector $\vec{S}$, an additional dial gauge is necessary, which measures on an edge perpendicular to the left edge. In the figure, this is the indicator whose probe tip rests on the point $P_3$ in the starting position. Analogous to the previous equation, the following applies in the end position for its probe tip point $R_3$:

$$\vec{R}_3 = \vec{Q}_3 + m_3\vec{D}_{34} = R(\alpha)\vec{P}_3 + \vec{S} + m_3\vec{D}_{34} \tag{13}$$

If the equations (12) and (13 ) are written by components for $x$ and $y$, they form a linear system of equations with four equations so that the four unknowns $S_x$, $S_y$, $m_2$ und $m_3$ can be calculated. This determines the desired displacement $\vec{S}$.

### 3.3.3 Shear forces on the buffers

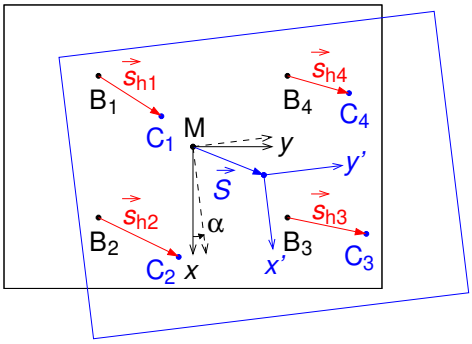


Figure 6: Horizontal distortion of the buffers

Fig. 6 shows how the buffers are stretched horizontally. In the initial position, which is marked by black color again, they are located in the points $B_n$. In the blue colored end position, their attachment points on the supporting plate are shifted to points $C_n$.

$$\vec{C}_n = R(\alpha)\vec{B}_n + \vec{S} \tag{14}$$

Shear forces then act on the buffers, which can be calculated using the horizontal extension distances $\vec{s}_{hn}$ and the buffer spring constant at shear $c_S$:

$$\vec{F}_{Sn} = c_S\vec{s}_{hn} = c_S \cdot (\vec{C}_n - \vec{B}_n) \qquad n = 1 \ldots 4 \tag{15}$$

The $x$-component of this force provides the force acting in the longitudinal direction on the respective buffer and the $y$-component the force acting in the transverse direction.

### 3.3.4 Compression forces on the buffers

The extent to which the supporting plate deflects in the vertical direction when inserting the VUT is also measured via dial gauges whose probe tips rest very close over the buffers. This allows the measured distances $s_{zn}$ to be equated approximately with the distances by which the buffers are compressed in the $z$-direction. The vertical forces on the buffers follow using the buffer spring constant $c$ under compressive load.

$$F_{zn} = c \cdot s_{zn} \qquad n = 1 \ldots 4 \tag{16}$$

# 4 Measurements in use

## 4.1 The test bench at Heilbronn University

The measurements are carried out on the test bench for electrified drives at Heilbronn University. At this test rig, a high-speed machine for direct tests of electric motors and two wheel load machines for tests on electric axles or single wheel drives are available. All three machines can also be used together, e.g. for tests of hybrid powertrains or transmission gearings. The electrical supply of the test sample is provided by a battery simulator. For the tests presented here, the two wheel load machines are employed. They each have a rated power of 120 kW. Their maximum speed is 2400 rpm and the maximum torque is 2000 Nm. They are also designed for high dynamics. The moment of inertia is less than 0.4 kgm$^2$. Rotational torque changes of up to 24000 Nm/s and speed changes of up to 30000 rpm/s can be achieved. With these data, the test bench is suitable for vehicle-in-the-loop tests of passenger cars from the A, B or C segment.

## 4.2 Static measurements during assembly

A small electric passenger car as a VUT is the first application for the supports. In order to determine the forces and torques on the vehicle mount in accordance with section 3.1, the movements of the supporting plate D are measured when the VUT is set up. To calculate the buffer forces, the spring constants of the buffers must be known. In order to verify the data sheet specifications, preliminary tests were carried out on the buffers. For this purpose, the buffers were subjected to pressure with defined weights and the compression was determined using dial gauges. Fig. 7 shows the measurement results.

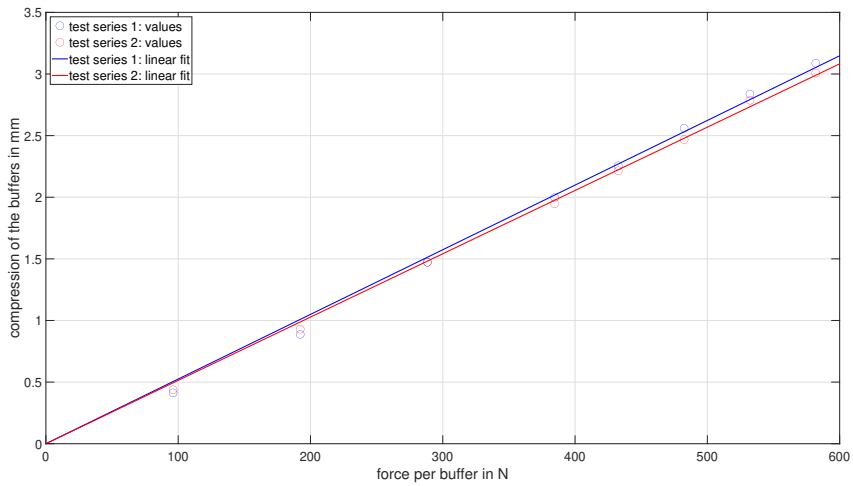


Figure 7: Measuring the spring constant in compression

This results in an average spring constant $c = 192.6$ N/mm.
A measurement was commissioned from the manufacturer of the buffers to determine the spring constant in shear. This resulted in a spring constant in shear $c_S = 30$ N/mm.
Table 2 shows the measurement results recorded by the dial gauges when the vehicle was inserted. $s_1 \ldots s_4$ are the recorded distances as a result of the horizontal movement of the supporting plate, see Fig. 5. $s_{z1} \ldots s_{z4}$ show the vertical movement of the plate at the four buffers. The vehicle was clamped twice. In the vertical direction, the plate moved similarly both times. The horizontal movement transverse to the direction of travel was also comparable. However, with respect to the $x$-axis, the plate moved differently. In the first mounting, it moved slightly against the direction of travel, while in the second mounting it moved noticeably in the direction of travel.
Table 3 shows the clamping forces and torques calculated using the measured movements when inserting the VUT. Depending on the mounting, the longitudinal force also varies in sign, which corresponds to the differences in the $x$-movement of the plate. The track torque $M_{sp}$ was always small, whereas the camber torque $M_{St}$ was pronounced. These results indicate a long service life of the support bearings of over 100 years. This is due to the low weight of the VUT, which belongs to the A segment. Axle weight and camber torque are the dominant factors influencing the service life of the supports. Based on values that are typical for vehicles from the C segment, the service life is approx. 10 years.

Table 2: Measured distances when inserting the VUT

| | $s_1$ (mm) | $s_2$ (mm) | $s_3$ (mm) | $s_4$ (mm) | $s_{z1}$ (mm) | $s_{z2}$ (mm) | $s_{z3}$ (mm) | $s_{z4}$ (mm) |
|---|---|---|---|---|---|---|---|---|
| 1st mounting | -0.50 | -0.20 | -0.13 | 0.01 | -4.24 | -3.38 | -1.61 | -2.10 |
| 2nd mounting | -0.10 | -0.27 | 0.74 | 1.07 | -4.09 | -3.45 | -1.68 | -2.03 |

Table 3: Clamping forces and torques

| | $F_v$ (N) | $F_l$ (N) | $F_q$ (N) | $M_{sp}$ (Nm) | $M_{st}$ (Nm) |
|---|---|---|---|---|---|
| 1st mounting | 2182 | 30 | 49 | -5.3 | -133.9 |
| 2nd mounting | 2167 | -104 | 24 | 5.5 | -135.7 |

Figure 8: VUT on test bench

### 4.3 Measurements with vehicle in driving mode

Fig. 8 shows the exemplary VUT, which is adapted to the wheel load machines with the help of the supports. This is a city car, which is assigned to class 2 due to its weak motorization with a power mass ratio $P_{mr} \leq 34$ W/kg. Fig. 9 illustrates the speed profile, which the WLTP standard [18] defines for this vehicle class. A test run according to this cycle on the test bench was accompanied with measurements using a 3-axis acceleration sensor mounted on the bearing block upper part. Fig. 10 shows the measurement results. The acceleration transverse to the direction of travel is somewhat more pronounced than that in the direction of travel, but always remains below 0.5 g and therefore low. In the vertical direction, it deviates from the acceleration due to gravity by a maximum of 0.13 g. The visual impression is that the vehicle runs smoothly and with only minor vibrations throughout the entire cycle.

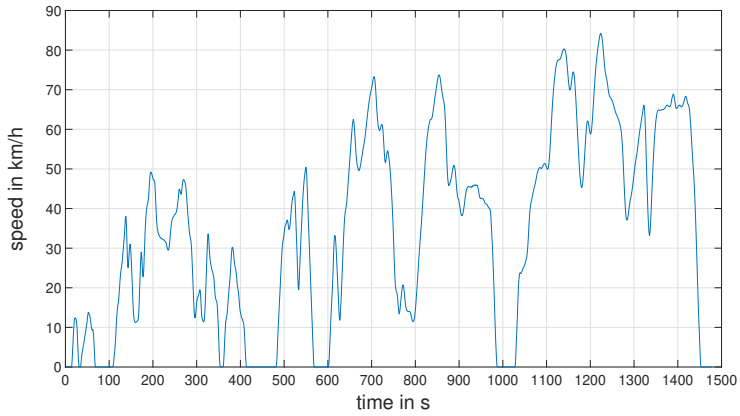


Figure 9: Speed profile of the WLTC for class 2 vehicles

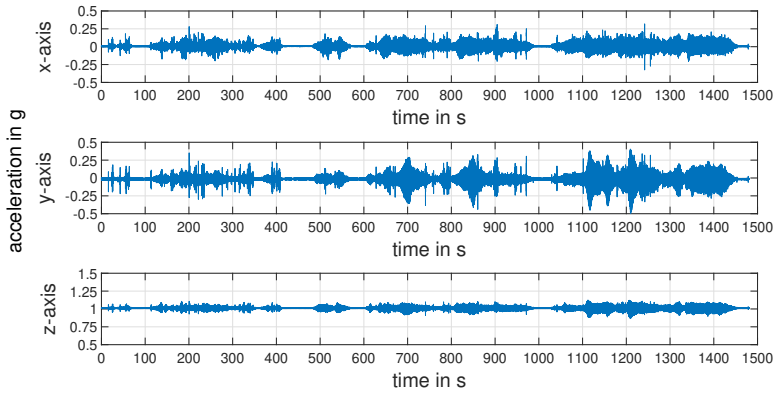


Figure 10: Measured accelerations on the bearing block upper part during WLTC

# 5 Conclusion

The first driving tests with an example vehicle adapted to the test bench show that the construction presented enables the safe operation of complete electric vehicles on the test bench. The space requirement is low and the vehicle can be mounted quickly thanks to the automatic alignment of the vehicle during insertion, both of which reduce costs. If the movement of the supporting plate is measured when the vehicle is inserted, the clamping forces and torques resulting from the mounting can be determined, which in turn allow a statement to be made about the bearing endurance. However, the measurement with dial gauges presented here requires care when positioning the dial gauges and adjusting their zero point, and the space for mounting all the necessary dial gauges at the same time is limited. An integrated electronic sensor system for displacement measurement could reduce the effort involved. In view of the costs, however, this was not done, so that in everyday practice a forecast of clamping forces and torques and the associated service life will not be made every time a new vehicle is adapted. With the lightweight example vehicle, the service life of the supports was very long. The supports offer sufficient reserve for accommodating cars up to the vehicle class for which the test bench is conceived.

# References

[1] M. Paulweber, K. Lebert. *Powertrain Instrumentation and Test Systems*, ISBN 978-3-319-32133-2, Springer, 2016.

[2] E. Schauer et al., *Development of Benchmarking Methods for Electric Vehicle Drive Units*, SAE Technical Paper 2024-01-2270, 2024, https://doi.org/10.4271/2024-01-2270.

[3] J. Cheng et al., *A Survey on Testbench-Based Vehicle-in-the-Loop Simulation Testing for Autonomous Vehicles: Architecture, Principle, and Equipment*, Advanced Intelligent Systems, 6(6), 2024, p. 2300778.

[4] B. Giechaskiel et al., *Experimental Comparison of Hub- and Roller-Type Chassis Dynamometers for Vehicle Exhaust Emissions*, Energies, 2022, 15(7), 2402. https://doi.org/10.3390/en15072402.

[5] C. Engström et al., *Considerations for Achieving Equivalence between Hub-and Roller-Type Dynamometers for Vehicle Exhaust Emissions*, Energies, 2022, 15(20), 7541. https://doi.org/10.3390/en15207541

[6] *A versatile test system (TS) for validating pure ice and electrified propulsion systems*, https://www.avl.com/en/testing-solutions/ice/hybrid-propulsion-testing/avl-powertrain-ts, accessed on 2024-08-14.

[7] M. Gießler et al., *Consumption-relevant load simulation during cornering at the vehicle test bench VEL*, In: 20. Internationales Stuttgarter Symposium: Automobil-und Motorentechnik, 2020, pp. 159-172, Springer Fachmedien Wiesbaden.

[8] M. H. Schmelzle et al., *Tire-force modeling on a hub-mounted vehicle-in-the-loop dynamometer while performing lateral maneuvers*, In: Autonomous Systems: Sensors, Processing, and Security for Ground, Air, Sea, and Space Vehicles and Infrastructure 2023, pp. 212-218, SPIE.

[9] Y. Goto et al., *Simulation wheel and vehicle testing apparatus*, European patent EP 2 187 193 B1, 2013.

[10] S. Weber, S. Egner. *Test wheel for a Drive Train Test Bench and Drive Train Test Bench*, International patent WO 2022/243105 A1, 2022.

[11] *Road-to-Rig- R2R 4x4 Test Rig*, https://www.pts-prueftechnik.de/en/expertiseservices/testing-on-test-rigs/road-to-rig-r2r-4x4-test-rig/, accessed on 2024-08-14.

[12] *Benefits of Dynapack*, https://dynapack.com/benefits-of-dynapack/, accessed on 2025-04-25.

[13] *ROTOTEST in Electrification applications*, https://rototest.com/applications/ev-electrification/, accessed on 2024-08-14.

[14] M. Lyashenko et al., *Analysis of ATV transmission operation according to the results of tests on a dynamometer test bench*, In: IOP Conference Series: Materials Science and Engineering, Vol. 820, No. 1, p. 012018, 2020, IOP Publishing.

[15] C. Engström et al., *Method and System for use in Dynamometer Testing of a Motor Vehicle*, European patent EP 3 635 360 B1, 2022.

[16] A. Daberkow, *Ein exploratives Lehrformat zur Elektromobilität im Kontext des forschungsorientierten Lernens*, In: Zeitschrift für Hochschulentwicklung, ISSN 2219-6994, Lustenau, Verein Forum neue Medien in der Lehre Austria, 2020, pp. 209-222.

[17] DIN ISO 281:2010-10, *Rolling bearings - Dynamic load ratings and rating life (ISO 281:2007)*.

[18] UN: Global Technical Regulation No. 15, *Worldwide harmonized Light vehicles Test Procedure*, ECE/TRANS/180/Add.15, 2014.

## Presenter Biography

Markus Harke received the diploma and Ph.D. degrees in electrical engineering from the Technical University of Munich (TUM), Germany, in 1995 and 2002, respectively. From 2001 to 2005, he was employed by Robert Bosch GmbH for the predevelopment of electric drives. In 2005 he joined the University of Applied Sciences Heilbronn (HHN) where he has been teaching as a professor in the Department of Mechanics and Electronics. His main research interest is in the field of electrical machines for applications with small to medium power and in electric traction drives.